Coherent control of the dynamics of a single quantum-dot exciton qubit in a cavity

Antonio de Freitas, L. Sanz, and José M. Villas-Bôas[*]
Instituto de Física, Universidade Federal de Uberlândia, 38400-902 Uberlândia, MG, Brazil
(Received 25 August 2016; revised manuscript received 9 January 2017; published 6 March 2017)

In this paper we demonstrate theoretically how to use an external laser field to control the population inversion of a single quantum dot exciton qubit in a nanocavity. We consider the Jaynes-Cummings model to describe the system, and the incoherent losses were taken into account by using Lindblad operators. We have demonstrated how to prepare the initial state in a superposition of the exciton in the ground state and the cavity in a coherent state. The effects of exciton-cavity detuning, the laser-cavity detunings, the pulse area, and losses over the qubit dynamics are analyzed. We also show how to use a continuous laser pumping in resonance with the cavity mode to sustain a coherent state inside the cavity, providing some protection to the qubit against cavity loss.

I. INTRODUCTION

Quantum information processing (QIP) has become one of the most promising applications of quantum mechanics [1,2]. The first criterion to be fulfilled for actual implementation of QIP [3,4] is the successful manipulation of a qubit, the basic unit for encoding quantum information [5]. In this context, manipulation means coherent control of the quantum dynamics of the chosen qubit. The density matrix formalism is the perfect tool [6] to explore those quantum dynamics, particularly when dealing with multipartite systems [7]. For open quantum systems, being in contact with a reservoir, this formalism provides a theoretical environment to describe the action of decoherence [8–10].

Since the general state of one qubit is defined as a quantum superposition on a two-dimensional basis, it is natural to describe it as a 1/2 spin system [2]. Coupling such a system with electromagnetic radiation is one of the paths to implement a coherent manipulation of the qubit, and the theoretical models to describe this interaction must take into the account the classical or quantum nature of the radiation [11]. When considering quantum radiation, the Jaynes-Cummings model [12] is one of the most successful theoretical descriptions of the spin-boson interaction and subsequent dynamics [13–15].

Thinking about physical implementations, semiconductor nanostructures have become potential candidates for applications in QIP and quantum computing [16,17]. Specifically, relevant contributions arise from the study of physical properties of quantum dots (QDs), often recognized as artificial atoms, in front of the discrete character of the energy spectrum due to the confinement of carriers [18,19]. A qubit can be encoded inside a QD by using the charge [20,21], the spin [22–25], as well as excitonic states [26–29] of the confined particle. One of the advantages of the QDs is the versatility on the experimental manipulation of the (valence-conduction) band gap, with the subsequent customization of its optical properties.

The unique characteristics of quantum states in a QD are behind the advantages of coupling a QD qubit with quantum light [30], particularly involving nanocavities [31]. Once the QDs are created using semiconductor materials, it is possible to confine carriers in order to maximize the dipole-dipole interaction, coupling the nanostructure strongly with a chosen mode of the electromagnetic field of the cavity [32,33]. The crescent interest on such an experimental setup lies on its potential for the miniaturization of the cavity quantum electrodynamics (CQED), as found in an atomic physics context [34]. Once a typical setup is smaller than a micrometer [22,30], one can consider the implementation of an *on-chip* CQED [35] using this kind of arrangement.

The rich optical response of quantum dots inside nanocavity includes nonlinearities [36] and nontrivial emission spectra [37,38]. Several groups concentrate efforts on developing applications of a QD-cavity setup such as quantum light emitters [39–43], exploring quantum dynamics in a similar way of successful procedures for production of quantum states of light in atomic CQED [44]. Another approach, directly related to QIP, is the use of quantum light for the coherent manipulation of the QD qubit. Typical phenomena of coherent dynamics such as Rabi oscillations [22,45,46], entanglement between a spin QD qubit and photons [47–49], and exciton-photon entanglement [50] have been observed on QD-cavity systems.

In this paper, we propose encoding a qubit using an excitonic state, interacting with a coherent state of light prepared in a nanocavity. The Jaynes-Cummings model is used to study the interaction between the quantum dot and the nanocavity and we consider photon losses in our treatment. We calculate the density matrix operator dynamics, once we are dealing with a multipartite open quantum system. Instead of a resonant condition between the quantum dot and the cavity [45], we assume a nonresonant, self-trapped dynamics.

To create and maintain a coherent state inside the cavity we use a continuous laser field applied in resonance with the cavity mode. To control the qubit rotations, the coherent manipulation of the system is done by applying external laser pulses. To find the best set of parameters for the coherent manipulation, we calculate the average occupation of the exciton state as a function of two detunings: laser-cavity and exciton-cavity. The effect of the pulse area is also evaluated and the residual effect of the pulses over the cavity state is surveyed by checking the average number of photons and photon distribution. We explore the behavior of the QD qubit by studying the population inversion, the dynamics over the Poincaré sphere, and the purity of the qubit, the last one using von Neumann entropy.

_____
[*]villas-boas@infis.ufu.br

II. THEORY

Our system is composed of a QD, treated here as a two-level system, coupled to a single mode nanocavity. To explore this physical setup, we use the Jaynes-Cummings model [12] under the rotating wave approximation (RWA) [38,51–53]. To model the external lasers we use the dipole and RWA approximations [11] and assume that the pulsed laser only interacts with the QD while the continuous laser only interacts with the cavity. The Hamiltonian can be written as ($\hbar = 1$)

$$
\begin{aligned}
H = {} & \omega_x \sigma_+ \sigma_- + \omega_c a^\dagger a + g(\sigma_+ a + \sigma_- a^\dagger) \\
& + \frac{\Omega(t)}{2}(e^{-i\omega_p t}\sigma_+ + e^{i\omega_p t}\sigma_-) \\
& + J(e^{-i\omega_l t}a^\dagger + e^{i\omega_l t}a),
\end{aligned} \tag{1}
$$

where $\sigma_\pm$ are the pseudospin operators for the QD exciton qubit; $a^\dagger$ and a are the creation and annihilation operators for photons inside the cavity; $\omega_x, \omega_c, \omega_p$, and ω_l are the frequencies of the exciton, cavity mode, pulsed laser, and continuous laser field, respectively; $\Omega(t) = \mu E(t)/\hbar$ is the Rabi frequency that describes the exciton-laser interaction, with μ being the electric dipole strength of the exciton transition and $E(t)$ the amplitude of the electric field of the laser, which can be constant or have different shapes in the pulsed excitation; and J contains information about the laser field amplitude and the cavity transmission coefficient.

We encode a quantum bit using the QD exciton state, $|0\rangle$ being the state with no exciton and $|1\rangle$ the exciton state, and the cavity is described by the usual Fock basis, $|n\rangle$. The Hamiltonian basis is depicted as $|i,n\rangle$ with $i = 0$ or 1, indicating the state of the QD qubit and n being the number of photons in the cavity.

To obtain the dynamics of our physical system, we numerically solved the time-dependent density matrix in the Lindblad form

$$
\frac{d\rho}{dt} = -\iota[H,\rho] + \kappa \mathcal{D}[a] + \gamma \mathcal{D}[\sigma_-] + \phi \mathcal{D}[\sigma_z] \tag{2}
$$

where H is the full Hamiltonian [Eq. (1)] and $\mathcal{D}[L] = L\rho L^\dagger - \frac{1}{2}(L^\dagger L\rho + \rho L^\dagger L)$ is the Lindblad superoperator, which contains the incoherent terms of the density matrix and assumes a Markovian approximation. Here κ is the photon loss rate of the cavity, γ is the decay rate of the QD, and ϕ is the pure dephasing rate of the QD.

In order to get a deeper understanding on the QD qubit dynamics we use the Poincaré-sphere representation, an analogy of the Bloch-sphere representation for mixed states [45]. The use of this representation is common in the context of cavity quantum electrodynamics [54]. The QD qubit treated here is not in a pure state: when losses are not considered (κ and γ null), the QD qubit is one of the parts of a bipartite system, and has some degree of entanglement with the cavity. In contrast, when considering losses, one can say the QD qubit exchanges just a portion of its information with the cavity, once the bipartite system is now open. To obtain the components X, Y, and Z of the Bloch vector we first compute the reduced density operator for the QD qubit by doing the partial trace over the cavity variables,

$$
\hat{\rho}^{\text{QD}} = \text{Tr}[\hat{\rho}]_{\text{cav}}, \tag{3}
$$

then

$$
\begin{aligned}
X &= 2\text{Re}(\hat{\rho}_{01}^{\text{QD}}), \\
Y &= 2\text{Im}(\hat{\rho}_{10}^{\text{QD}}), \\
Z &= \hat{\rho}_{00}^{\text{QD}} - \hat{\rho}_{11}^{\text{QD}}.
\end{aligned} \tag{4}
$$

On the Poincaré sphere, the Z component of the mixed Block-like vector coincides with the population inversion. The value of the azimuthal angle is known as the relative phase which corresponds to ϕ in the pure qubit represented as $C_0|0\rangle + e^{i\phi}C_1|1\rangle$, with C_i being related to the population of the state $|i\rangle$. A Bloch vector with a null azimuthal angle lies on the YZ plane [2].

To quantify the purity of the QD qubit, we use the von Neumann entropy S, which is defined as [2]

$$
S(\hat{\rho}^{\text{QD}}) = -\text{Tr}[\hat{\rho}^{\text{QD}} \log_2(\hat{\rho}^{\text{QD}})]. \tag{5}
$$

From the definition, $S = 0$ indicates that the QD qubit is a pure system, described by a state separated from the cavity and the reservoir. If losses are not considered on the description of the system, the maximal degree of entanglement between the qubit with the cavity corresponds to $S = 1$.

III. RESULTS AND DISCUSSION

To analyze the dynamics of a QD qubit we parametrize all frequencies in units of g, so it is easy to convert the values obtained here to real experimental situations. For example, in a photonic crystal nanocavity $\hbar g$ is of the order of 0.1 meV [38]. This parametrization also allows our results to be applied to other cavity systems, which we will not discuss here. To solve the time-dependent master equation we carefully choose the size of the photon basis to describe accurately the cavity state according to its mean occupation, taking into account the effects of interaction between the QD, cavity, and external lasers. In most of the cases studied, a Fock basis of $n_{\max} = 70$ was sufficient, so we set this value for all simulations presented here.

To get some insight into what we can do, let us first ignore the incoherent effect ($\kappa, \gamma, \phi = 0$) and consider the initial state of our system as a direct product of a coherent state $|\alpha\rangle$ in the cavity and the QD in the ground state $|0\rangle$, thus $|\Psi(0)\rangle = |0\rangle |\alpha\rangle$. The coherent state can be represented in the basis of Fock states as

$$
|\alpha\rangle = \exp(-|\alpha|^2/2) \sum_n \frac{\alpha^n}{\sqrt{n!}} |n\rangle, \tag{6}
$$

where $|\alpha|^2 = \langle n \rangle$ is the mean number of photons. A coherent state in the cavity can be created by sending a laser in resonance with the cavity mode for a short period of time ($J \neq 0$ and $\omega_j = \omega_c$ in our Hamiltonian).

Figure 1 illustrates several aspects of the QD qubit dynamics when interacting with the cavity without the action of any external laser field ($J, \Omega = 0$) and neglecting the incoherent effect ($\kappa, \gamma, \phi = 0$). We consider that the exciton state is resonant with the cavity mode, $\delta_x = \omega_x - \omega_c = 0$, and an initial cavity state with $\langle n \rangle = 25$. Figure 1(a) shows the behavior of the population inversion, $Z(t)$, with the apparition of collapses and revivals around an average value $\langle Z \rangle = 0$,
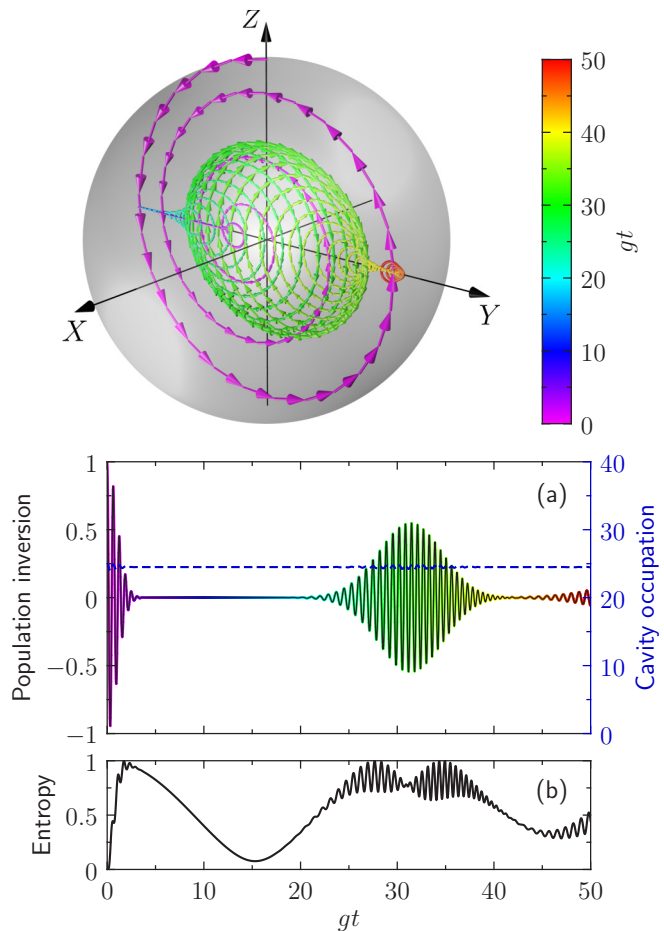
FIG. 1. Dynamics of a QD qubit inside a cavity considering full resonant condition given by $\delta_x = 0$ and in the absence of lasers fields. (a) Population inversion and cavity occupation (dashed blue line) as a function of gt. (b) Von Neumann entropy as a function of gt. Upper panel shows the evolution of a QD qubit over the Poincaré sphere.
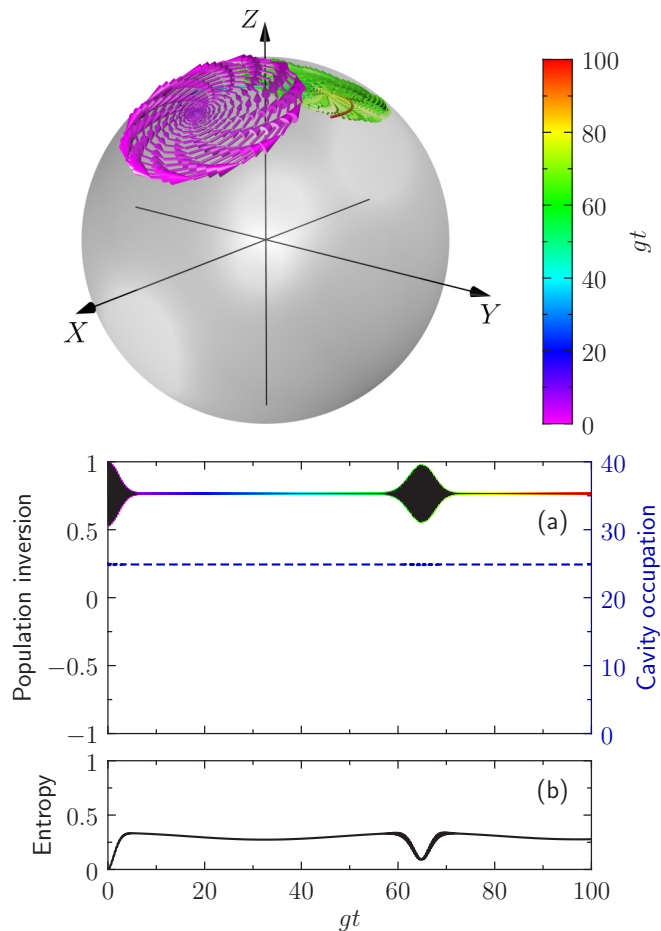

FIG. 2. Dynamics of a QD qubit inside a cavity considering nonresonant condition with $\delta_x = -18g$ and in the absence of lasers fields. (a) Population inversion and cavity occupation (dashed blue) as a function of gt. (b) Von Neumann entropy as a function of gt. Upper panel shows the evolution of a QD qubit over the Poincaré sphere.

in agreement with the predictions of the Jaynes-Cummings model. Notice that the average occupation of the cavity stays almost constant at a value around $\langle n \rangle \simeq 25$.

The dynamics of the QD qubit on the Poincaré sphere is shown in the upper panel of Fig. 1, illustrated by constructing a vector the components of which are defined by Eq. (4). In this figure, a scale of colors and arrows helps to visualize the temporal evolution. First, the QD qubit starts from the pure state $|0\rangle$, indicated by the purple curves at the north pole of the Poincaré sphere. Then, at short times, the QD qubit performs a rotation around the X axis, which is restricted to the YZ plane ($X = 0$), showing that the relative phase is null under the evolution. It is also observed that the norm shrinks as time increases, which becomes evident at long times, as shown by green, yellow, and red arrows.

The QD qubit dynamics restricted to a small region inside the Poincaré sphere is connected with a high degree of entanglement with the cavity. This behavior is better understood by checking the evolution of the von Neumann entropy $S(\hat{\rho}_{QD})$, Eq. (5), shown in Fig. 1(b). The initially pure QD qubit ($S = 0$ at $gt = 0$) performs oscillations between high and low entangled states, with an almost complete purification at

$gt \simeq 15$ associated with the collapse on population inversion. This behavior repeats subsequent collapses (not shown). As time further increases, the degree of entanglement increases and approaches the maximal entangled states indicated by $S(\hat{\rho}_{QD}) \simeq 1$.

It is also important to explore the behavior of the system under a nonresonant condition between the QD qubit and cavity. Figure 2 shows the same theoretical tools used on the description of the QD qubit resonant dynamics but considering $\delta_x = -18g$. Figure 2(a) shows that the population inversion does not perform complete oscillations between the QD qubit states, although collapses and revivals around the average value $\langle Z \rangle \simeq 0.75$ are still present. This phenomenon is called *self-trapping* or population trapping and is a well-known aspect of nonresonant dynamics concerning two-level systems. The average occupation of the cavity stays constant at the value of $\langle n \rangle = 25$ over the evolution as seen by the blue line linked to the right axis. The self-trapping is more evident in the upper panel of Fig. 2, once the mixed state vector is confined in a restricted region on the north hemisphere of the Poincaré sphere. It is worth noting that the mixed
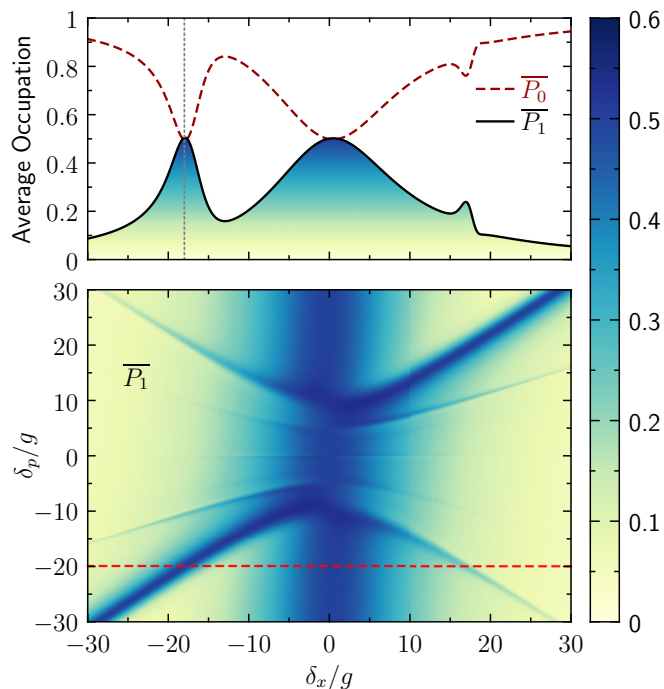
FIG. 3. Lower panel: False color plot of the average occupation of the exciton states $\overline{P_1}$ after the system being prepared in the state $|\Psi(0)\rangle = |0\rangle\,|\alpha\rangle$ for a constant laser with $\Omega = 2g$ as functions of detunings $\delta_x = \omega_x - \omega_c$ and $\delta_p = \omega_p - \omega_c$ with $J = 0$. Dark regions correspond to energy configurations where the qubit exciton state $|1\rangle$ is being populated. Dashed red line illustrates the condition $\delta_p = -20g$, where individual average occupations are shown in the upper panel. Dotted gray line in the upper panel corresponds to $\delta_x = -18g$, being the best condition for population inversion.

vector performs rotations around the Z axis. Thinking in terms of a general qubit state written as $|\Psi\rangle = C_0\,|0\rangle + e^{i\phi}C_1\,|1\rangle$, changes in the relative phase ϕ are connected with changes with the value of the azimuthal angle of the qubit Bloch vector. Thus, the nonresonant dynamics brings a gain of relative phase of the mixed vector, which oscillated between zero and 2π. Figure 2(b) shows the von Neumann entropy, where differently from Fig. 1 the entanglement of the QD qubit suffers a stabilization, having an asymptotic value around $S \simeq 0.3$. Notice also that an increase of the purification appears at the revival of oscillations in the population inversion, indicating that the system tries to recover its initial state. In general, the nonresonant condition preserves the purity of the QD qubit, once it prevents the qubit from interacting in an efficient way with the cavity.

After checking the basic aspects of QD qubit-cavity dynamics, we are ready to understand the action of the external lasers and incoherent effects. The main problem here is to find the right parameters to send the laser pulses as the coupling between the QD and cavity modifies its interaction with the laser. A practical and fast way to survey the effect of this new ingredient can be done through calculations of the average occupation $\overline{P_{i,n}} = \lim_{\tau\to\infty} \frac{1}{\tau}\int_0^\tau P_{i,n}(t)dt$ of basis states $|i,n\rangle$ as a function of some physical parameters neglecting incoherent process and assuming a constant laser excitation [$\Omega(t)$ constant], which allows us to use the time-independent

Schrödinger equation to compute the time evolution. As we are interested in the qubit dynamics and want to investigate where the population inversion occurs, we write the average occupation of the ith QD qubit state as $\overline{P_i} = \sum_n \overline{P_{i,n}}$. Here we choose to seek the best exciton-cavity $\delta_x = \omega_x - \omega_c$ and laser-cavity $\delta_p = \omega_p - \omega_c$ detunings and the reason for this choice is that the cavity frequency ω_c is usually fixed by construction, making our procedure very similar to what one would do in an experimental setup.

Figure 3 (lower panel) shows the average occupation of the exciton state as functions of δ_x and δ_p for our system under a constant laser excitation with $\Omega = 2g$ interacting with the QD, keeping $J, \kappa, \gamma, \phi = 0$. The initial state is again $|\Psi(0)\rangle = |0\rangle\,|\alpha\rangle$ with $\langle n \rangle = 25$. Bright regions indicate low population of the exciton state in opposition to dark areas, therefore, dark areas are good candidates for laser induced population inversion. In the upper panel of Fig. 3 we show a cut in the false color plot for $\delta_p = -20g$ (red dashed line in the lower panel), showing the average occupation of the two QD qubit components. Gray dotted lines at $\delta_x = -18g$ indicate the maximum value of $\overline{P_1}$, being a good candidate to present a high degree of population inversion under pulsed excitation.

In order to gain a fine control of the dynamics in realistic situations, we check the effect of the pulse parameters more closely. We proceed with the simulations using a single Gaussian pulse of duration $gt_p = 0.7$, which in a typical strong-coupled QD-cavity system would be a pulse with duration of the order of 4 to 5 ps, centered at $gt_p = 10$,
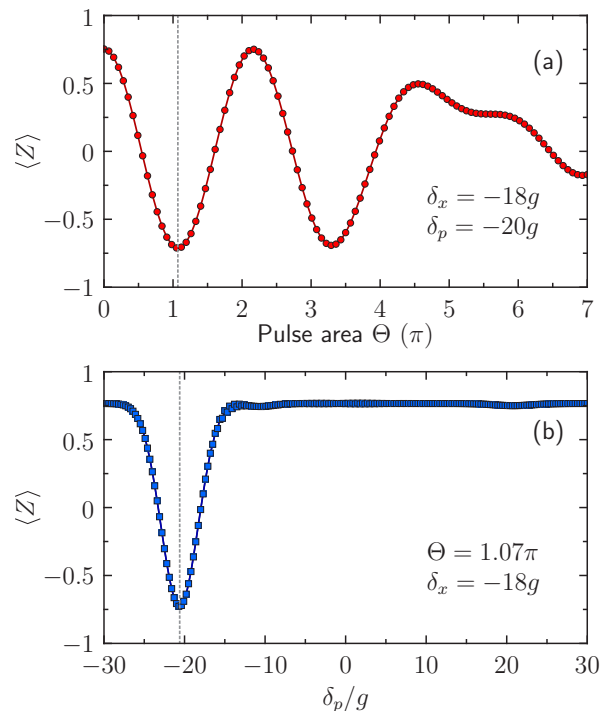

FIG. 4. (a) Average of the population inversion $\langle Z \rangle$ as a function of the pulse area Θ after the application of a single Gaussian pulse at $gt_1 = 10$ with duration of $gt_p = 0.7$ and detunings $\delta_x = -18g$ and $\delta_p = -20g$. (b) Average of the population inversion $\langle Z \rangle$ as a function of δ_p for a pulse with same parameters as in (a) with an area $\Theta = 1.07\pi$.

with optimal parameters obtained from Fig. 3 ($\delta_x = -18g$ and $\delta_p = -20g$). We observed that the average of the population inversion $\langle Z \rangle$ after the pulse is strongly dependent on the pulse area, defined as $\Theta = \int_{-\infty}^{\infty} \Omega(t)dt$, as we can see in Fig. 4(a). The maximum change in $\langle Z \rangle$ is obtained for $\Theta \simeq 1.07\pi$ and 3.3π. The dependence of $\langle Z \rangle$ with Θ shows that the self-trapped dynamics, initially fixed at some polar angle over the Poincaré sphere, can be set up on demand by the action of a prearranged laser pulse. It is interesting to note that high values of the pulse area bring nonlinear effects, linked with the increase of the pulse intensity and resulting in a lack of control of the dynamics. This is indicated by nontrivial values of $\langle Z \rangle$ for $\Theta > 4$.

We now simulate the behavior of $\langle Z \rangle$ as a function of the laser detuning to the cavity frequency considering a laser pulse with area $\Theta = 1.07\pi$, corresponding to the first minimum in Fig. 4(a). As we can see in Fig. 4(b), $\langle Z \rangle$ changes drastically for values around $\delta_p = -20g$, in accord with the predictions for the continuous laser as shown in Fig. 3. It is also interesting to notice that there is a dip of $\langle Z \rangle$ around $\delta_p = -20.6g$, in a range of $\approx 5\delta_p$, meaning the effects of the pulse on dynamics permits some flexibility over the exact value of δ_p. For practical applications, once we establish an adequate value of δ_p (using the survey of populations), a specific pulse can be set up on demand in order to perform controlled self-trapped dynamics of the QD qubit. This set of parameters, $\delta_x = -18g$, $\delta_p = -20.6g$, and $\Theta \simeq 1.07\pi$, will be kept constant for the rest of the paper.

To corroborate our approach, we proceed to explore the dynamics of population inversion, QD qubit on the Poincaré sphere, and von Neumann entropy. We discuss the action of a sequence of three pulses. We consider again the QD qubit initialized at the ground state $|0\rangle$ and the cavity in the coherent state $|\alpha\rangle$ with $\langle n \rangle = 25$ and the conditions described before.

Figure 5 shows the QD qubit dynamics under the action of a sequence of three pulses, all with duration of $gt_p = 0.7$ for the best detuning found before. The format of the pulse is shown in Fig. 5(a). The population inversion, Fig. 5(b), shows that the QD qubit initially (for $gt < 5$) performs self-trapped oscillations around $\langle Z \rangle \simeq 0.75$. This can be better visualized in the top panel of Fig. 5, where the dynamics is restricted to the north hemisphere of the Poincaré sphere. After the application of the first pulse at $gt_1 = 5$ with pulse area $\Theta_1 = 1.07\pi$, the population inversion starts an oscillation with a new structure of collapses and revivals, oscillating around $\langle Z \rangle \simeq -0.73$, still in a self-trapped dynamics as can also be seen in the Poincaré sphere, moving the oscillation from the north to the south hemisphere. After the application of the second pulse at $gt_2 = 10$ with the same pulse area $\Theta_2 = 1.07\pi$, the self-trapping oscillations change to an average value around $\langle Z \rangle \simeq 0.72$, moving back to the north hemisphere of the Poincaré sphere. Further control can be obtained with the last pulse, applied at $gt_3 = 15$ with a pulse area of half of the previous case ($\Theta_3 = 1.07\pi/2$), creating a superposition between exciton and ground state, showing that we can control the QD qubit state reasonably well with this choice of pulse sequence. Concerning the entanglement dynamics, again explored using the von Neumann entropy plotted in Fig. 5(b), it is worth noting that the first two pulses change slightly the entanglement degree of the QD qubit, keeping
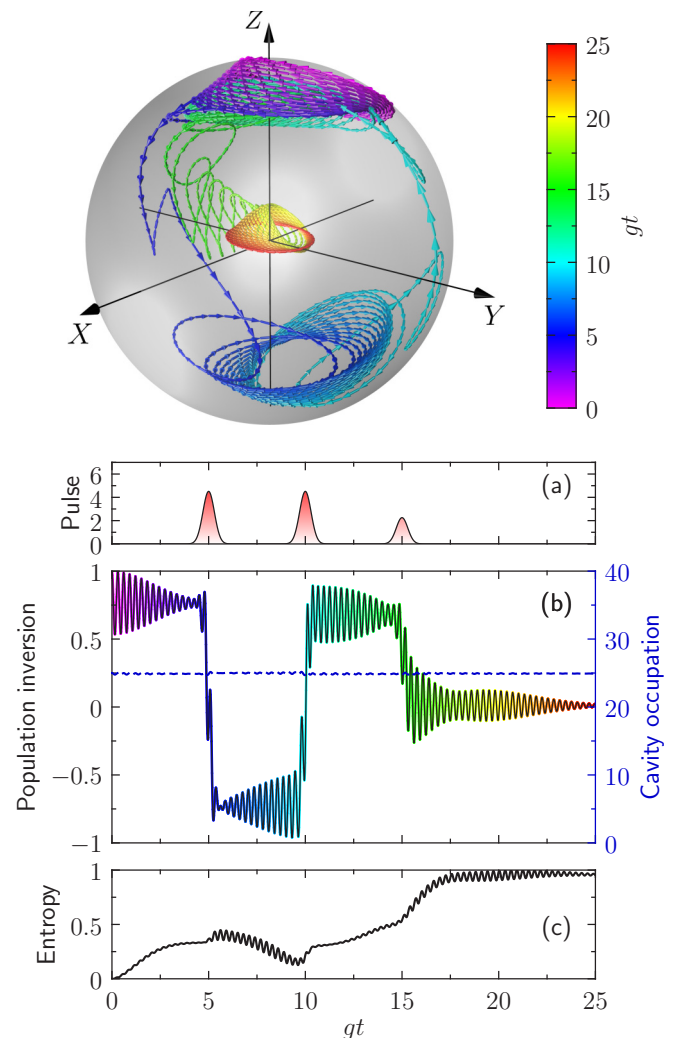

FIG. 5. Dynamics of a QD qubit inside a cavity considering $\delta_x = -18g$, $\delta_p = -20.6g$, neglecting losses and under the effect of three Gaussian pulses, the first and second with the same pulse area $\Theta = 1.07\pi$, and the last with $\Theta = 1.07\pi/2$, applied at $gt_1 = 5$, $gt_2 = 10$, and $gt_3 = 15$, all with duration of $gt_p = 0.7$. (a) Sequence of pulses used in the simulation. (b) Population inversion and cavity occupation (dashed blue) as a function of gt. (c) Von Neumann entropy as a function of gt. Upper panel shows the evolution of a QD qubit over the Poincaré sphere, with the color code and arrows indicating the time sequence.

the value of the entropy below 0.5. The third pulse, on the other hand, creates a situation similar to the full resonant case, Fig. 1, where the entropy goes to maximum, and the inversion exhibits oscillations around the average value of $\langle Z \rangle = 0$.

One advantage of using the nonresonant condition is that the QD lifetime increases from a few hundred picoseconds to a few nanoseconds due to the reduction of fluctuations in the vacuum of the electromagnetic field [33]. Taking the lower limit, let us assume that the lifetime of the QD is about 0.7 ns, which gives a decay rate of the order of $\gamma = 0.01g$. Since we are proposing the manipulation the QD qubit in a time scale of a few picoseconds, the effects of this decay rate can be neglected in our analysis. We also consider a pure dephasing rate of the same order of magnitude $\phi = 0.01g$ and, as we
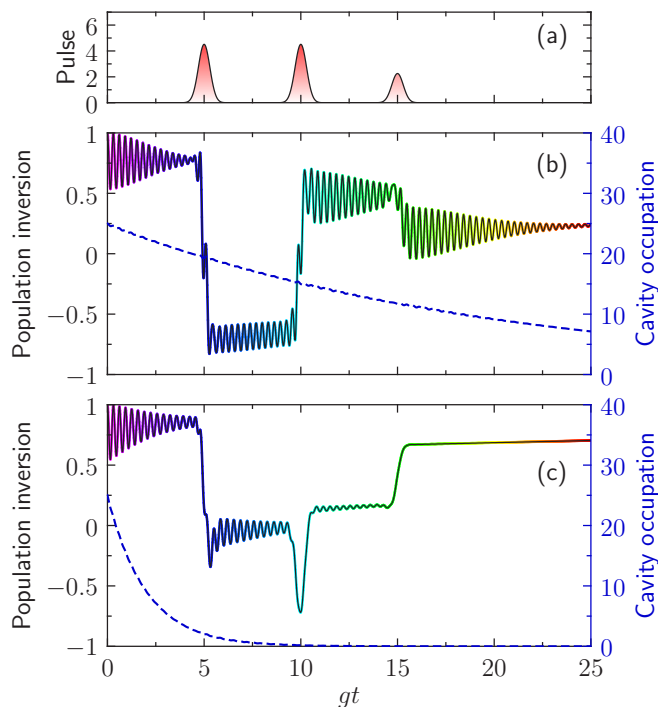
FIG. 6. Dynamics of a nonresonant QD qubit inside a cavity under the effect of three Gaussian pulses for the same set of parameters used in Fig. 5, but now considering decoherence. (a) Sequence of pulses used in the simulation. (b) Population inversion and cavity occupation (dashed blue line) as a function of gt for $\kappa = 0.05g$, $\gamma = 0.01g$, and $\phi = 0.01g$. (c) Same as (b) for $\kappa = 0.5g$.

shall see later, pure dephasing plays an important role in the preparation of the initial state used in dynamics of the coupled system.

Cavity loss is another term that cannot be neglected since the average life span of a photon within a cavity may be as small as a few picoseconds in a bad cavity. To understand the effects of the cavity loss, in Fig. 6 we show the dynamics of the system using the same parameters and sequence of pulses as in Fig. 5, but now including incoherent effects. In Fig. 6(b) we use $\gamma = 0.01g$, $\phi = 0.01g$, and $\kappa = 0.05g$, while in Fig. 6(c) we use $\gamma = 0.01g$, $\phi = 0.01g$, and $\kappa = 0.5g$. As we can see in this figure, even a small loss of the cavity is enough to break the QD qubit manipulation. Notice that the average occupation of the cavity photons decreases exponentially and we have $\langle n \rangle \simeq 20$, 15, and 12 when the first, second, and third pulses are applied, respectively. Pure dephasing and exciton spontaneous decay plays no role in this particular case as the time scale is small. Notice that we have used ($|\Psi(0)\rangle = |\alpha\rangle |0\rangle$) as the initial state, which is a pure state. For the case of $\kappa = 0.5g$, Fig. 6(c), the occupation of the cavity goes to zero very quickly, being zero before the second pulse, and the coherent manipulation of the QD qubit is completely destroyed. Thus, even though the cavity is out of resonance, the loss of the cavity plays an important role in the QD qubit manipulation.

It is important to mention that the coherent state under cavity loss will still be a coherent state, but with a lower average of photons. The main problem here is that the resonance condition (the best parameter we found in Figs. 3

and 4) changes over time as the photon population decreases and a complete control of the QD state will require a previous evaluation of the best parameter for each pulse of the pulse sequence to control its states. Experimentally, this is challenging, as it requires sending pulses with different frequencies and intensities in a short time scale.

To solve this problem, instead of using the laser described by the coupling J to only prepare the initial coherent state in the cavity, let us keep it as a constant pump to maintain a steady coherent state in the cavity. In Fig. 7 we plot the evolution of the photon distribution in the Fock basis considering $\delta_x = -18g$, $\delta_p = -20.6g$, (same parameters used before), $\omega_j = \omega_c$, $J = 1.28g$, $\kappa = 0.5g$, $\gamma = 0.01g$, and $\phi = 0.01g$ as a function of gt, assuming $|\Psi(0)\rangle = |0\rangle |0\rangle$ as the initial state. Here we choose $j = 1.28g$ because that produces a steady coherent state with $\langle n \rangle \simeq 25.3$, close to the condition used in Fig. 5. The right panel is a view of the photon distribution for $gt = 100$, showing a coherent photon distribution.

Using the state at $gt = 100$ obtained with $J = 1.28g$ as the initial state of the system, in Fig. 8 we show the dynamics of the system under the same pulse sequence and parameters as in Fig. 6(c), with additional parameters $\omega_j = \omega_c = 0$, $\kappa = 0.5g$, $\gamma = 0.01g$, and $\phi = 0.01g$. As we can see in Fig. 8(b), we have now a better control of the inversion of population with our pulse sequence as the cavity occupation is kept almost constant over the evolution despite the application of the laser pulses interacting with the QD. The value is very close to our ideal situation (with no losses), with an average of photons in the cavity around $\langle n \rangle \simeq 25$ as we initially planed. Notice, however, that the range of population inversion is decreased; this is due to the pure dephasing rate acting in the preparation of the state of the cavity (the evolution during the pulse sequence is too short for the pure dephasing and decay of the exciton to play a role). The effect of the pure dephasing rate in the initial state can also be seen in Fig. 8(c), where the initial value of the von Neumann entropy is about 0.6. Despite the
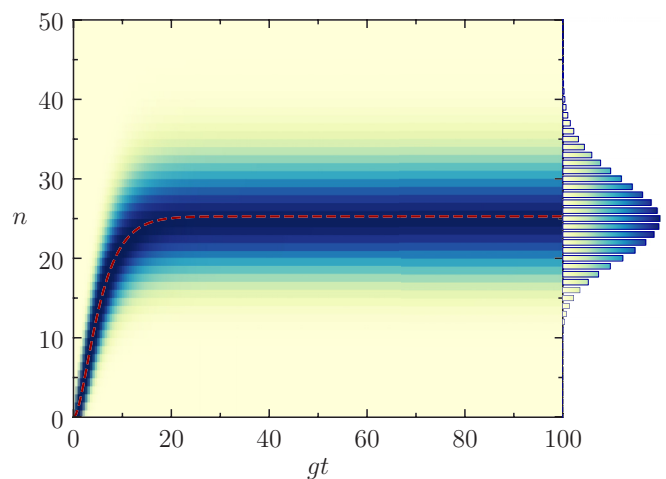

FIG. 7. (a) Evolution of the photon distribution in the cavity for $\kappa = 0.5g$, $\gamma = 0.01g$, $\phi = 0.01g$, and $J = 1.28g$ assuming $|\Psi(0)\rangle = |0\rangle |0\rangle$ as initial state. Right panel shows the photon distribution for the quantum state at $gt = 100$.
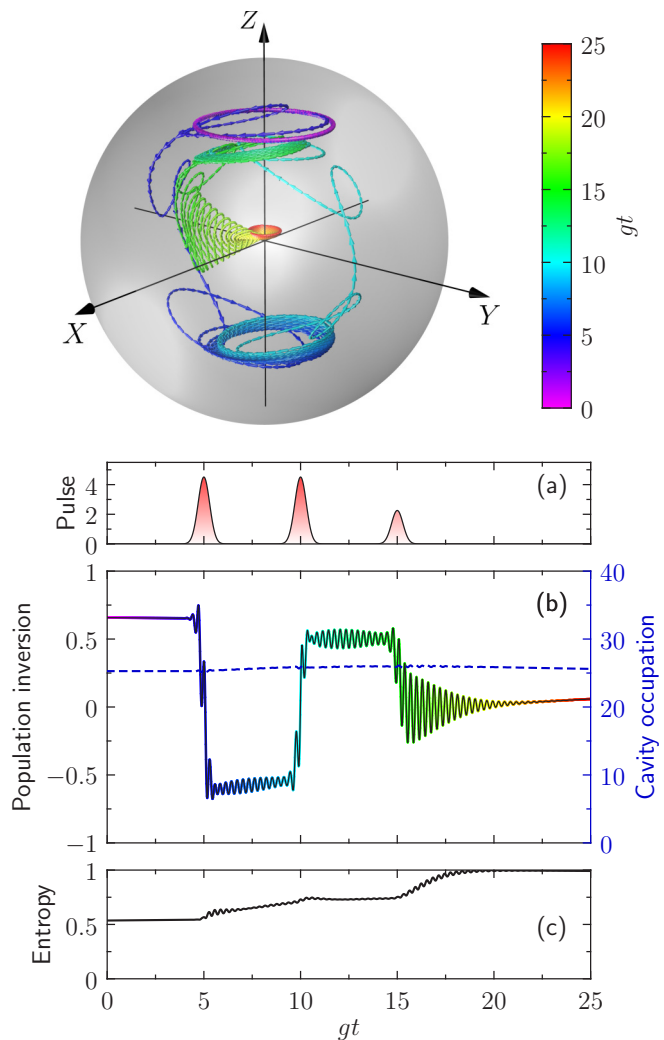
FIG. 8. Dynamics of a QD qubit inside a cavity under the effect of three Gaussian pulses as in Fig. 5, now considering $\kappa = 0.5g$, $\gamma = 0.01g$, $\phi = 0.01g$, and $J = 1.28g$ and the initial state the state at $gt = 100$, the photon distribution of which is shown in the right panel of Fig. 7. (a) Sequence of pulses used in the simulation. (b) Population inversion and cavity occupation (dashed blue line) as a function of gt. (c) Von Neumann entropy as a function of gt. Upper panel shows the evolution of a QD qubit over the Poincaré sphere, with the color code indicating the time sequence.

initial difference, the evolution of the von Neumann entropy is very similar to the case analyzed previously in Fig. 5(c).

Neglecting pure dephasing completely and keeping all parameters as in Fig. 8 we obtain Fig. 9. These two figures have similar general characteristics. The main differences are in the range of the population inversion and the initial value of the von Neumann entropy, which is a result of the different initial state as we mentioned above. In the case with pure dephasing, Fig. 8(b), the population inversion is restricted to smaller absolute values, resulting in self-trapping close to the central region of the Poincaré sphere, indicating that we have a mixed state. This results in a large value of the von Neumann entropy, indicating that the initial state prepared (Fig. 7 for $gt = 100$) is not pure. Here it is important to mention that pure dephasing in solid-state systems cannot be neglected,
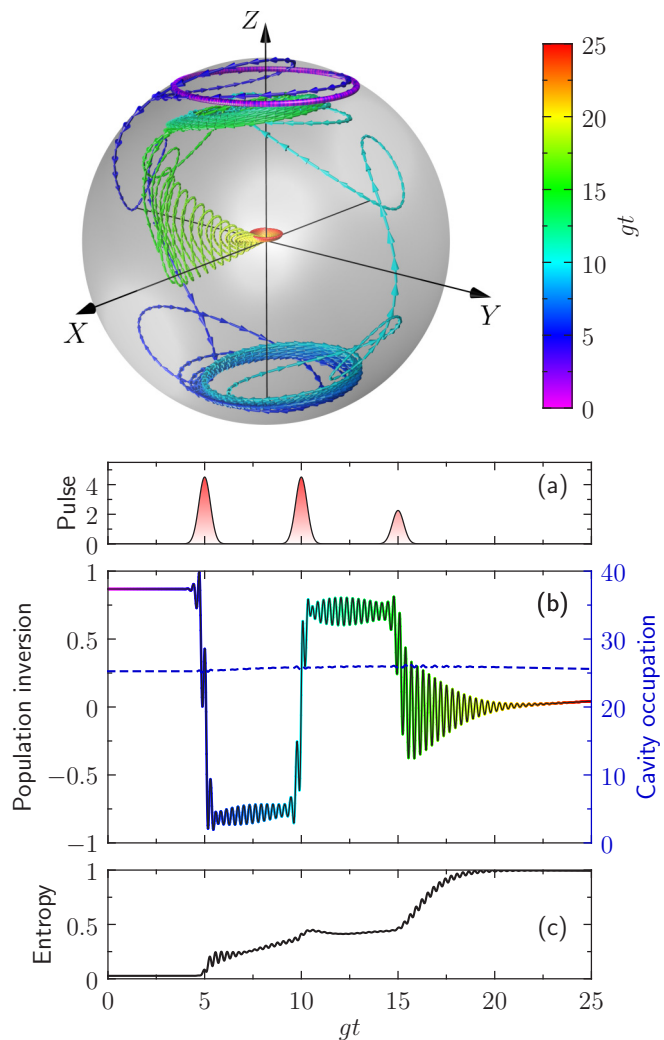

FIG. 9. Dynamics of a QD qubit inside a cavity under the effect of three Gaussian pulses and parameters as in Fig. 8, now neglecting pure dephasing and considering the initial state as the state at $gt = 100$ for $\phi = 0.0$. (a) Sequence of pulses used in the simulation. (b) Population inversion and cavity occupation (dashed blue line) as a function of gt. (c) Von Neumann entropy as a function of gt. Upper panel shows the evolution of a QD qubit over the Poincaré sphere, with the color code indicating the time sequence.

being always present due to the nature of the system and the presence of phonons; in this way, the preparation of the initial state in a solid-state system will always face this problem. To minimize its effect, the exciton-cavity detuning can be increased. In systems where pure dephasing can be safely neglected, the result presented in Fig. 8 might be useful.

IV. SUMMARY

In this paper, we discuss the dynamics of an exciton in a quantum dot which interacts with a coherent state, supported by a cavity, under the action of a continuous laser, for controlling the cavity losses, and external Gaussian laser pulses, to control exciton-cavity dynamics. Our study is a step towards the implementation of an *on-chip* cavity quantum electrodynamics. We define a qubit using two levels on the

quantum dot so $|0\rangle$ is the vacuum state (no exciton) and $|1\rangle$ is the exciton state (QD qubit). We use the population inversion, $Z(t)$, and a mixed vector definition of a QD qubit on the Poincaré sphere to study the system dynamics. We also use the von Neumann entropy to analyze the entanglement degree (closed system) and the degree of purity (open system) between the qubit and the cavity mode.

The treatment without considering losses provides important information: the average population is used to define an efficient condition of qubit-cavity and pulse-cavity detunings for populating the dressed states $|i,n\rangle$. The dynamics shows self-trapping on population inversion, with oscillations of the relative phase of the qubit. By including the pulses, we check the effect of the pulse area on the dynamics, showing that the central value of population inversion changes significantly after the pulse. The sequence of pulses can be also used to increase the entanglement degree between the qubit and the cavity in the nonresonant ideal (no losses) condition.

We also discuss the effect of losses on our approach. Because the QD qubit lifetime is long enough (and it can be even longer in a nonresonant condition with the cavity), we avoid the effects of spontaneous emission by choosing a short time scale defined by $gt < 25$. The QD qubit dynamical control, on demand, is attained by using a sequence of short pulses. To protect the manipulation against cavity losses,

we explore the use of an additional continuous laser, which maintains a steady coherent state inside the cavity. This mechanism already sustains the QD qubit dynamics, assuring the success of our proposal. We also analyzed the effects of pure dephasing of the QD qubit in the dynamics, showing that it produces no effects in the time evolution during our short pulse sequence, but it might affect the preparation of the initial state.

In future papers, we intend to continue studying the entanglement between the QD qubit and cavity by quantifying the existence of quantum correlations when considering losses. The goal is to explore the potential of this system as an entanglement resource. A second issue is to engage a study about production quantum light but with a focus other than single photons.

[1] K. M. Svore and M. Troyer, Computer **49**, 21 (2016).

[2] M. A. Nielsen and I. L. Chuang, *Quantum Computation and Quantum Information* (Cambridge University, Cambridge, England, 2000).

[3] D. P. DiVincenzo, Science **270**, 255 (1995).

[4] C. H. Bennett and D. P. DiVincenzo, Nature (London) **404**, 247 (2000).

[5] B. Schumacher, Phys. Rev. A **51**, 2738 (1995).

[6] U. Fano, Rev. Mod. Phys. **29**, 74 (1957).

[7] C. Cohen-Tannoudji, B. Diu, and F. Laloë, *Quantum Mechanics* (Wiley, New York, 1992).

[8] M. Schlosshauer, Rev. Mod. Phys. **76**, 1267 (2005).

[9] W. H. Zurek, Rev. Mod. Phys. **75**, 715 (2003).

[10] A. P. Alivisatos, Science **271**, 933 (1996).

[11] M. O. Scully and M. S. Zubairy, *Quantum Optics* (Cambridge University, Cambridge, England, 1997).

[12] E. Jaynes and F. Cummings, Proc. IEEE **51**, 89 (1963).

[13] B. W. Shore and P. L. Knight, J. Mod. Opt. **40**, 1195 (1993).

[14] J. Larson, Phys. Scr. **76**, 146 (2007).

[15] A. D. Greentree, J. Koch, and J. Larson, J. Phys. B **46**, 220201 (2013).

[16] B. E. Kane, Nature (London) **393**, 133 (1998).

[17] L. C. L. Hollenberg, A. S. Dzurak, C. Wellard, A. R. Hamilton, D. J. Reilly, G. J. Milburn, and R. G. Clark, Phys. Rev. B **69**, 113301 (2004).

[18] G. Burkard, D. Loss, and D. P. DiVincenzo, Phys. Rev. B **59**, 2070 (1999).

[19] D. Loss and D. P. DiVincenzo, Phys. Rev. A **57**, 120 (1998).

[20] G. Shinkai, T. Hayashi, T. Ota, and T. Fujisawa, Phys. Rev. Lett. **103**, 056802 (2009).

[21] T. Hayashi, T. Fujisawa, H. D. Cheong, Y. H. Jeong, and Y. Hirayama, Phys. Rev. Lett. **91**, 226804 (2003).

[22] W. Gao, A. Imamoğlu, H. Bernien, and R. Hanson, Nat. Photon. **9**, 363 (2015).

[23] D. Press, T. D. Ladd, B. Zhang, and Y. Yamamoto, Nature (London) **456**, 218 (2008).

[24] J. Petta, A. Johnson, J. Taylor, E. Laird, A. Yacoby, M. Lukin, C. Marcus, M. Hanson, and A. Gossard, Science **309**, 2180 (2005).

[25] A. Imamoğlu, D. D. Awschalom, G. Burkard, D. P. DiVincenzo, D. Loss, M. Sherwin, and A. Small, Phys. Rev. Lett. **83**, 4204 (1999).

[26] P. Chen, C. Piermarocchi, and L. J. Sham, Phys. Rev. Lett. **87**, 067401 (2001).

[27] X. Li, Y. Wu, D. Steel, D. Gammon, T. H. Stievater, D. S. Katzer, D. Park, C. Piermarocchi, and L. J. Sham, Science **301**, 809 (2003).

[28] J. E. Rolon and S. E. Ulloa, Phys. Rev. B **82**, 115307 (2010).

[29] J. M. Villas-Bôas, A. O. Govorov, and S. E. Ulloa, Phys. Rev. B **69**, 125342 (2004).

[30] J. L. O'Brien, A. Furusawa, and J. Vučković, Nat. Photon. **3**, 687 (2009).

[31] K. J. Vahala, Nature (London) **424**, 839 (2003).

[32] Y. Akahane, T. Asano, B.-S. Song, and S. Noda, Nature (London) **425**, 944 (2003).

[33] K. Hennessy, A. Badolato, M. Winger, D. Gerace, M. Atature, S. Gulde, S. Falt, E. L. Hu, and A. Imamoğlu, Nature (London) **445**, 896 (2007).

[34] S. Haroche, Rev. Mod. Phys. **85**, 1083 (2013).

[35] P. Lodahl, S. Mahmoodian, and S. Stobbe, Rev. Mod. Phys. **87**, 347 (2015).

[36] M. P. Bakker, T. Ruytenberg, W. Löffler, A. Barve, L. Coldren, M. P. van Exter, and D. Bouwmeester, Phys. Rev. B **91**, 241305 (2015).

[37] A. Majumdar, M. Bajcsy, A. Rundquist, E. Kim, and J. Vučković, Phys. Rev. B **85**, 195301 (2012).

[38] A. Laucht, N. Hauke, J. M. Villas-Bôas, F. Hofbauer, G. Böhm, M. Kaniber, and J. J. Finley, Phys. Rev. Lett. **103**, 087405 (2009).

[39] K. Müller, A. Rundquist, K. A. Fischer, T. Sarmiento, K. G. Lagoudakis, Y. A. Kelaita, C. Sánchez Muñoz, E. del Valle, F. P. Laussy, and J. Vučković, Phys. Rev. Lett. **114**, 233601 (2015).

[40] D. Heinze, D. Breddermann, A. Zrenner, and S. Schumacher, Nat. Commun. **6**, 8473 (2015).

[41] C. S. Muñoz, E. Del Valle, A. G. Tudela, K. Müller, S. Lichtmannecker, M. Kaniber, C. Tejedor, J. Finley, and F. Laussy, Nat. Photon. **8**, 550 (2014).

[42] T. Farrow, P. See, A. Bennett, M. Ward, P. Atkinson, K. Cooper, D. Ellis, D. Unitt, D. Ritchie, and A. Shields, Nanotechnology **19**, 345401 (2008).

[43] A. Kiraz, M. Atatüre, and A. Imamoğlu, Phys. Rev. A **69**, 032305 (2004).

[44] S. Deleglise, I. Dotsenko, C. Sayrin, J. Bernu, M. Brune, J.-M. Raimond, and S. Haroche, Nature (London) **455**, 510 (2008).

[45] C. Dory, K. A. Fischer, K. Müller, K. G. Lagoudakis, T. Sarmiento, A. Rundquist, J. L. Zhang, Y. Kelaita, and J. Vučković, Sci. Rep. **6**, 25172 (2016).

[46] J. Reithmaier, G. Sęk, A. Löffler, C. Hofmann, S. Kuhn, S. Reitzenstein, L. Keldysh, V. Kulakovskii, T. Reinecke, and A. Forchel, Nature (London) **432**, 197 (2004).

[47] K. De Greve, L. Yu, P. L. McMahon, J. S. Pelc, C. M. Natarajan, N. Y. Kim, E. Abe, S. Maier, C. Schneider, M. Kamp *et al.*, Nature (London) **491**, 421 (2012).

[48] J. R. Schaibley, A. P. Burgers, G. A. McCracken, L.-M. Duan, P. R. Berman, D. G. Steel, A. S. Bracker, D. Gammon, and L. J. Sham, Phys. Rev. Lett. **110**, 167401 (2013).

[49] W. B. Gao, P. Fallahi, E. Togan, A. Delteil, Y. S. Chin, J. Miguel-Sanchez, and A. Imamoğlu, Nat. Commun. **4**, 2744 (2013).

[50] M. Müller, S. Bounouar, K. D. Jöns, M. Glässl, and P. Michler, Nat. Photon. **8**, 224 (2014).

[51] P. L. Knight and L. Allen, Phys. Rev. A **7**, 368 (1973).

[52] A. Brown, W. J. Meath, and P. Tran, Phys. Rev. A **63**, 013403 (2000).

[53] E. K. Irish, Phys. Rev. Lett. **99**, 173601 (2007).

[54] N. Kalb, A. Reiserer, S. Ritter, and G. Rempe, Phys. Rev. Lett. **114**, 220501 (2015).